Multimodal Sensor Medical Image Fusion Based on Type-2 Fuzzy Logic in NSCT Domain

Yong Yang, *Member, IEEE*, Yue Que, Shuying Huang, *Member, IEEE*, and Pan Lin

***Abstract*—Multimodal medical image fusion plays a vital role in different clinical imaging sensor applications. This paper presents a novel multimodal medical image fusion method that adopts a multiscale geometric analysis of the nonsubsampled contourlet transform (NSCT) with type-2 fuzzy logic techniques. First, the NSCT was performed on pre-registered source images to obtain their high- and low-frequency subbands. Next, an effective type-2 fuzzy logic based fused rule is proposed for fusion of the high-frequency subbands. In the presented fusion approach, the local type-2 fuzzy entropy is introduced to automatically select high-frequency coefficients. However, for the low-frequency subbands, they were fused by a local energy (LE) algorithm based on the corresponding image's local features. Finally, the fused image was constructed by the inverse NSCT with all composite subbands. Both subjective and objective evaluations showed better contrast, accuracy, and versatility in the proposed approach compared to state-of-the-art methods. Besides, an effective color medical image fusion scheme is also given in the paper that can inhibit color distortion to a large extent and produce an improved visual effect.**

***Index Terms*—Medical image, multimodal sensor fusion, nonsubsampled contourlet transform, type-2 fuzzy logic, fuzzy entropy.**

I. Introduction

THE continual development of medical imaging and information processing technologies provides many types of medical images for clinical diagnosis. The images are widely used in disease diagnosis, surgery, and radiation therapy [1], [2]. However, the obtained sensor responses of different modalities of medical images convey different information about the human body, organs, and cells, and have their own uses. For example, computed tomography (CT) images can depict dense structures like bones and hard tissue with less distortion, while magnetic resonance imaging (MRI) images is better visualized in the case of soft tissues [3]. Similarly, T1-MRI images provide anatomical structure details of tissues, while T2-MRI images provide information about normal and pathological tissues [4]. Positron emission tomography (PET) images can provide functional eloquent brain regions such as motor or speech regions by using specific activation tasks. In addition, single-photon emission computed tomography (SPECT) images reveal clinically significant metabolic change. Therefore, single sensor image often cannot provide enough information to doctors in actual clinical situations. It is usually necessary to combine the sensor images of different modalities to obtain more comprehensive information on diseased tissue or organs. An effective combining method is to use image fusion technologies, which can automatically combine multimodal sensor medical images [5]. The fused image not only obtains a more accurate and complete description of a target, but also reduces randomness and redundancies produced by the sensor in the image. Image fusion increases the effectiveness of image-guided diagnoses and the assessment of medical problems [6].

Image fusion methods can be divided into three levels from low to high, based on their information representation: pixel-level, feature-level and decision-level [7]. Pixel-level image fusion is performed directly on the original acquired image, retaining most of its detail information [8]. Hence, most current research and applications pertain to pixel-level image fusion. Generally, those algorithms are divided into two categories, spatial domain based and transform domain based [9]. Spatial domain techniques are carried out directly on source images using local spatial features. However, pixel-level spatial domain algorithms usually lead to several undesirable side effects, including reduced contrast [10].

Currently, the transform domain based multiscale image fusion algorithm has become a mainstream fusion method [11]. The traditional gradient pyramid (GP) transform and discrete wavelet transform (DWT) have been used successfully in image fusion [12], [13]. However, those transforms lack shift invariance due to their underlying down-sampling process [14], which means the fusion is sensitive to registration. To overcome these shortcomings of DWT, Kingsbury [15] proposed the dual-tree complex wavelet transform (DTCWT), an over-complete wavelet transform that provides both good shift invariance and directional selectivity. However, the DTCWT

This work is supported by the National Natural Science Foundation of China (No. 61262034, No. 61462031 and No. 61473221), by the Natural Science Foundation of Jiangxi Province (No. 20151BAB207033), by the Young Scientist Foundation of Jiangxi Province (No. 20122BCB23017), by the Fundamental Research Funds for the Southeast University (No. CDLS-2015-05), by the Nature Science Foundation of Shaanxi Province of China (No. 2015JM3105), and by the Project of the Education Department of Jiangxi Province (No. KJLD14031, No. GJJ150461 and No. GJJ150438).

Y. Yang, and Y. Que are with the School of Information Technology, Jiangxi University of Finance and Economics, Nanchang 330032, China (e-mail: greatyangy@126.com; qki120@163.com).

S. Huang is with the School of Software and Communication Engineering, Jiangxi University of Finance and Economics, Nanchang 330032, China (e-mail: shuyinghuang2010@126.com).

Pan Lin is with Key Laboratory of Child Development and Learning Science (Southeast University), Ministry of Education, Nanjing 210096, China and with Key Laboratory of Biomedical Information Engineering of Education Ministry, Institute of Biomedical Engineering, Xi'an Jiaotong University, Xi'an 710049, China(e-mail: tiger.lin9906@gmail.com).

constructed by 2-D wavelet that is isotropic and cannot effectively describe abrupt transitions such as line and curve singularities. In addition, the wavelet can only be limited to capture three directions of the information [16]. To overcome the shortcomings of the wavelet, Do and Vetterli developed a true 2-D image representation method in 2002; namely, the contourlet transform (CT) [17]. Compared with DWT, the CT has not only multiscale parameters and localization but also multi-direction and anisotropy. As a result, the CT can render edges and other singularities along curves more efficiently [18]. However, the up and down-sampling process of CT results in a lack of shift invariance and the presence of pseudo-Gibbs phenomena in the fusion. In 2006, A. L. D. Cunha *et al*. proposed an over complete transform, namely, the nonsubsampled CT (NSCT) [19]. The NSCT inherits the advantages of the CT while also possessing shift-invariance and effectively suppressing pseudo-Gibbs phenomena [20]. Thus, the NSCT is more suitable for image fusion.

The key problem in the transform domain based fusion algorithm is the selection of the fusion rules. For low-frequency coefficients, the simplest way is to carry a weighted average of the coefficients. However this rule decreases contrast in the fused images [21] and cannot result in high quality fused sub-images for medical purposes. For high-frequency coefficients, the popular method is to use a larger absolute rule to select fused coefficients, but that rule does not consider the association between the corresponding coefficients [22].

In recent years, soft computing technology, especially various aspects of fuzzy logic theory, have been successfully applied to image processing [23]–[26]. Because of their peculiarity of modeling uncertainty, fuzzy logic-based image fusion methods usually yield better performance than classic image fusion methods. Fuzzy logic is applied as either a feature transform operator or a decision operator for image fusion [9], [27]. The optimal membership function and fuzzy set selection is an open problem in image fusion. The effects of feature processing and analysis can be improved by combining fuzzy logic and multifarious analysis approaches. In the research of the past two decades, there has been increasing interest in higher order forms of fuzzy logic; in particular, the application of type-2 fuzzy logic techniques. For example, type-2 fuzzy logic has been successfully applied to image segmentation [28], edge detection [29], classification [30], quality assessment [31] and noise removal [32]. However, they are seldom used for image fusion. Compared with traditional fuzzy logic, the membership functions in type-2 fuzzy logic are also fuzzy, and this extra degree of fuzziness allows better management of higher degrees of uncertainty.

In this paper, a novel fusion framework based on the NSCT and type-2 fuzzy logic is proposed for multimodal sensor medical images. The core contribution of the method lies in the proposed fusion rule. The type-2 fuzzy logic techniques are unified as the high-frequency subbands fusion rules in which the local type-2 fuzzy entropy is employed to select the fused coefficients for intelligent decision-making. For the low-frequency subbands fusion rule was constructed by local energy (LE) based on the characteristics of human visual system (HVS). The combination of these two rules can reserve more details of source images and thus increase the quality of the fused images. Further, the proposed framework is also extended for color fusion in YUV color space, which can integrate more information and contrast enhancement than the existing schemes because it fully utilizes human color perception. The presented fusion method was applied to different clinically obtained multimodal sensor medical images and compared with popular fusion methods from the literatures. The experimental results indicated that the proposed method can obtain better subjective and objective results than a series of existing fusion methods.

The rest of this paper is organized as follows: The related theories are briefly introduced in Section II. The proposed image fusion method is described in Section III. The experimental results and analysis are depicted in Section IV, and the conclusions are given in Section V.

II. Related work

Theories related to the proposed fusion method are introduced in this section. These concepts, including the NSCT and type-2 fuzzy set, are briefly described as follows.

A. Nonsubsampled contourlet transform

The CT process is divided into two stages, and offers an efficient directional multi-resolution image representation. First, the Laplacian pyramid (LP) is used to capture the point singularities and used to decompose the original images into low- and high-frequency sub-images. Then, a directional filter bank (DFB) produces an efficient directional multiresolution image representation and divides the high-frequency subbands into directional subbands [17]. A contourlet decomposed schematic diagram is shown in Fig. 1(a). According to the sampling theorem, the pseudo-Gibbs phenomena would appear in low- and high-frequency sub-images in LP domain. Directional sub-

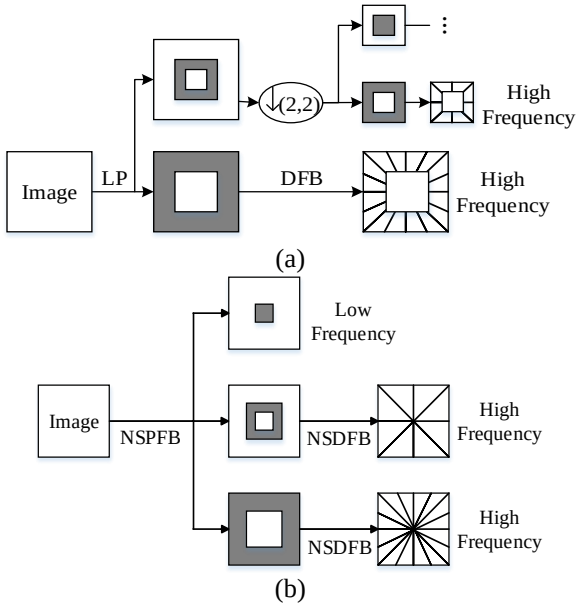

Fig. 1. (a) A contourlet decomposed schematic diagram. (b) A nonsubsampled contourlet decomposed schematic diagram.

bands which come from the high frequency sub-images by DFB filtering would also appear the pseudo-Gibbs phenomena.

To solve this problem, A. L. D. Cunha *et al*. proposed NSCT based on the theory of CT. The whole implementation of the NSCT process consists of two phases, multiscale decomposition and directional decomposition [19]. The major difference from the CT is that the NSCT is composed of two shift invariant parts, nonsubsampled pyramid filter banks (NSPFB) and nonsubsampled directional filter banks (NSDFB). An NSCT decomposed schematic diagram with $k = 2$ levels is shown in Fig. 1(b). The size of different sub-images decomposed by NSCT is identical, so it is easy to find the connection among sub-images of different images, which is beneficial to design fusion rules. Additionally, NSCT-based image fusion can effectively reduce the impacts of mis-registration on the results.

B. Type-2 fuzzy sets

The fuzzy set theory created by Zadeh [33] effectively solves the fuzziness problem which is difficult to solve using classic mathematics. However, because conventional (type-1) fuzzy set membership functions are determined, it is not flexible, so it is difficult to minimize uncertainty effects by using any kind of membership function and algorithm. In practical applications, the membership function is usually defined based on intuition empirically with a high degree of subjectivity. Therefore, the main difference lies in that the defined membership functions differ from one fuzzy processing technology to another on the same problem [34]. To solve the above problems, Zadeh proposed a generalized fuzzy set; namely, a type-2 fuzzy set. In the type-2 fuzzy set, the element membership relationship is uncertain and fuzzy, so does the membership function. Hence, a type-2 fuzzy set can describe the elements of uncertainty and the fuzzy membership function of uncertainty.

A type-2 fuzzy set usually can be defined as

$$A = \{((x,u), \mu_A(x,u)) \mid \forall x \in X, \forall u \in J_x \subseteq [0,1]\}, \quad (1)$$

where A denotes the type-2 fuzzy set, and $\mu_A(x,u)$ denotes its type-2 membership function with $0 \le \mu_A(x,u) \le 1$. J_x denotes the primary membership function and $\mu_A(x',u)$ denotes the secondary membership function when $x = x'$.

However, the type-2 fuzzy set is more complex than the type-1 fuzzy set, requiring more calculation. Secondly, the choice of secondary membership function is also a problem. In practical applications, a simplified type-2 fuzzy set is often used, namely the interval type-2 fuzzy set. In the interval type-2 fuzzy set [35], the membership of the element is defined on a given interval and the value of any point on the interval is one ($\mu_A(x,u) = 1$). This may be expressed in mathematical terms as

$$A = \{((x,u),1) \mid \forall x \in X, \forall u \in J_x \subseteq [0,1]\}, \quad (2)$$

An alternative definition of an interval type-2 fuzzy set may be obtained by utilizing type-1 membership functions

$$A = \begin{cases} (x, \mu_L(x), \mu_U(x)) \mid \forall x \in X \\ \mu_L(x) \le \mu(x) \le \mu_U(x) \mid u \in [0,1] \end{cases}, \quad (3)$$

where A denotes the interval type-2 fuzzy set, $\mu(x)$ denotes the initial type-1 fuzzy membership function, and $\mu_L(x)$ and $\mu_U(x)$ denote the lower and upper membership functions of the interval type-2 fuzzy set A. The lower and upper membership functions correspond to the lower and the upper envelopes of the interval type-2 membership function and can be obtained by the fuzzy type-1 membership function. In practical applications, it is usual to take one pair of reciprocal parameters to characterize as follows:

$$\begin{cases} \mu_L(x) = [\mu(x)]^{\alpha} \\ \mu_U(x) = [\mu(x)]^{(1/\alpha)} \end{cases}, \quad (4)$$

where parameter α serves as a fuzzy linguistic hedge with $\alpha \ge 1$. Actually, good results can be obtained when $\alpha \in [1,2]$. A type-2 fuzzy set and a frame type-1 fuzzy set on the control of the relationship can be represented using the footprint of uncertainty (FOU). The term FOU is used in the literature to express the shape of a type-2 fuzzy set [34]. The construction of a type-2 fuzzy set from a skeleton type-1 membership function and the FOU associated with the constructed type-2 fuzzy set are show in Fig. 2. The FOU implies that a distribution exists on top of the shaded area.

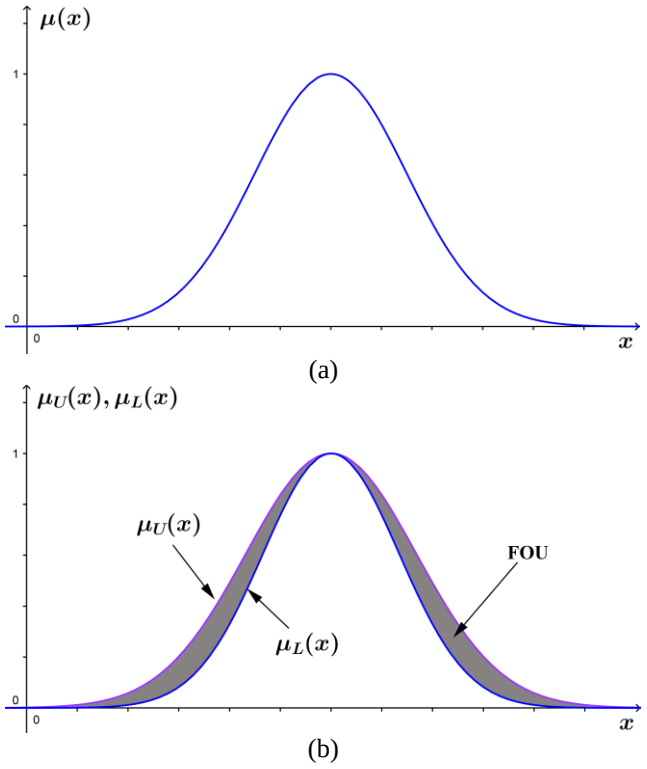

Fig. 2. Membership functions. (a) Type-1 Gaussian membership function. (b) Type-2 interval Gaussian membership function with its lower and upper membership functions, which are constructed from type-1 membership functions. The shaded area between the upper and lower membership functions is the FOU.

III. PROPOSED METHOD

This section provides a more detailed description of the proposed fusion method in NSCT domain. Suppose A and B are two registered source images. After *k*-level NSCT decomposition, a series of high-frequency subbands at each level and direction, while one low-frequency subband can be obtained;

This article has been accepted for publication in a future issue of this journal, but has not been fully edited. Content may change prior to final publication. Citation information: DOI 10.1109/JSEN.2016.2533864, IEEE Sensors Journal

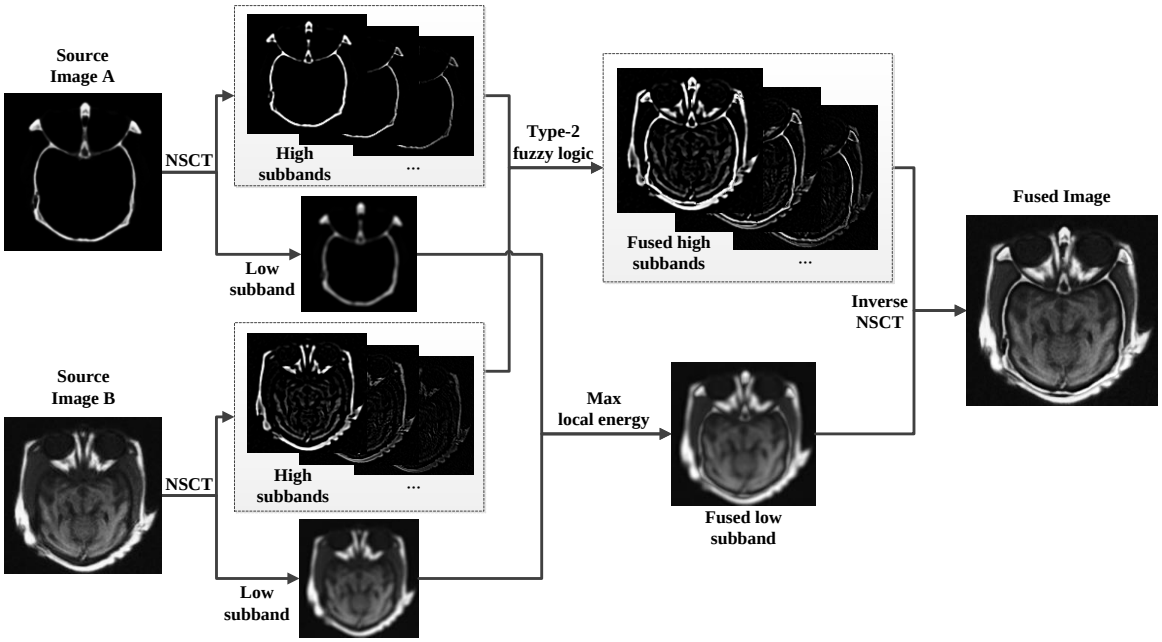

Fig. 3. The framework of the proposed fusion algorithm.

i.e., A: $\{H_{k,l}^{A}, L^{A}\}$ and B: $\{H_{k,l}^{B}, L^{B}\}$, where $H_{k,l}^{A}$ and $H_{k,l}^{B}$ are the high-frequency sub-images at level k and direction l, while L^{A} and L^{B} are the low-frequency sub-images. The fusion rules for these subband images decomposed by the NSCT are very important for the quality of the fusion [36].

A. *Fusion rule for high-frequency sub-images*

Inside the NSCT transform, high-frequency sub-images generally represent the detailed components of the source images, such as edges, textures, and region boundaries. At present, max absolute fusion rule is often used in a high-frequency domain. This method ignores the correlation among neighboring pixels and is sensitive to noise, which can easily be mistaken for useful information in the fused image. Hence, a new criterion is proposed here based on type-2 fuzzy logic, which takes full advantage of local image information and can effectively extract the details of an image to make an intelligent decision on the selection of high-frequency coefficients.

Based on an interval type-2 fuzzy set, each high-frequency subband is represented by a type-2 fuzzy set. First, the shape of the skeleton membership function $\mu(x)$ is chosen as follows:

$$\mu_{k,l}^{I}(i,j) = \frac{1}{1+\left|\frac{H_{k,l}^{I}(i,j)-c}{a}\right|^{2}}, \tag{5}$$

where $I = (A, B)$ and (i, j) denotes the spatial location of the high-frequency coefficient in the subband. Here, c = average($H_{k,l}^{I}$) and a = min($H_{k,l}^{I}$). Next, at each position of the membership function values of the lower and upper membership functions $\mu_L(x)$ and $\mu_U(x)$ are calculated as follows:

$$\begin{cases} \mu_L^{I,k,l}(x,y) = [\mu_{k,l}^{I}(i,j)]^{\alpha} \\ \mu_U^{I,k,l}(x,y) = [\mu_{k,l}^{I}(i,j)]^{(1/\alpha)} \end{cases}. \tag{6}$$

If a sub-image is considered as a fuzzy set, then the degree of fuzziness of a sub-image is a key factor affecting the performance of the determination of the fused coefficients for the image fusion framework. Fuzzy entropy was first proposed in 1968 by Zadeh and is a measure of the degree of fuzziness of a fuzzy set [37]. Currently, fuzzy entropy has become a very important concept in the theory of fuzzy systems. According to information theory, the larger the fuzzy entropy of a fuzzy set, the more information the fuzzy set has [38]. Therefore, when the fuzzy set has the maximum fuzzy entropy, the corresponding sub-image coefficients is the best fused coefficients.

The fuzzy entropy of an interval type-2 fuzzy set has been a popular research topic [39]–[41]. In this paper, we use an improved definition of the fuzzy entropy of an interval type-2 fuzzy set as follows [42]:

$$E(A) = \sum_{x_i \in X'} (A^{+}(x_i) - A^{-}(x_i)) + \sum_{x_i \in X/X'} \frac{\min(A^{-}(x_i), 1 - A^{+}(x_i))}{\max(A^{-}(x_i), 1 - A^{+}(x_i))}, \tag{7}$$

where $A^{+}(x_i)$ and $A^{-}(x_i)$ denote the lower and upper membership functions of an interval type-2 fuzzy set A, $X' = \{x_i \mid A^{-}(x_i) < 0.5 < A^{+}(x_i), i = 1, 2, ..., n\}$. Expanding it to a 2D image plane, the introduction of local type-2 fuzzy entropy is as follows:

$$E_{k,l}^{I}(i,j) = \sum_{(x,y)\in X'} (\mu_U^{I,k,l}(x,y) - \mu_L^{I,k,l}(x,y)) + \sum_{(x,y)\in X/X'} \frac{\min(\mu_L^{I,k,l}(x,y), 1 - \mu_U^{I,k,l}(x,y))}{\max(\mu_L^{I,k,l}(x,y), 1 - \mu_U^{I,k,l}(x,y))}, \tag{8}$$

where $X = \{(x,y) \mid x = 0,1,...,M-1, y = 0,1,...,N-1\}$ denotes a window of size $M \times N$ centered on the high-frequency coefficients and

$$X' = \{(x,y) \mid \mu_L^{I,k,l}(x,y) < 0.5 < \mu_H^{I,k,l}(x,y), \; x = 0,1,...,M-1, y = 0,1,...,N-1\}. \tag{9}$$

This article has been accepted for publication in a future issue of this journal, but has not been fully edited. Content may change prior to final publication. Citation information: DOI 10.1109/JSEN.2016.2533864, IEEE Sensors Journal

Therefore, the fused high-frequency coefficient $H_{k,l}^{F}(i,j)$ follows the fusion rule

$$H_{k,l}^{F}(i,j)=\begin{cases} H_{k,l}^{A}(i,j), & E_{k,l}^{A}(i,j)\geq E_{k,l}^{B}(i,j) \\ H_{k,l}^{B}(i,j), & otherwise \end{cases} . \quad (10)$$

B. Fusion rule for low-frequency sub-images

The coefficients in the low-frequency sub-images represent the approximation component and contain most of the energy of the source images. The simplest way to produce the composite bands is to use conventional averaging methods. However, that way cannot produce a fused low-frequency component for high quality medical images because it leads to reduced contrast in the fused images. The HVS is not sensitive to a single pixel, but is sensitive to changes in the local neighborhoods of pixels. Hence, we use the LE to construct fusion rules to make full use of the corresponding image's local features. The LE is defined by following equation:

$$LE^{I}(L^{I}(i,j))=\frac{1}{M\times N}\sum_{m=1}^{M}\sum_{n=1}^{N}L^{I}(i+m,j+n)^{2} , \quad (11)$$

where $I=(A,B)$, (i,j) denotes the spatial location of the low-frequency coefficient in the subband, and $(M\times N)$ is the window size.

Therefore, the fused low-frequency coefficient $L^{F}(i,j)$ follows the fusion rule:

$$L^{F}(i,j)=\begin{cases} L^{A}(i,j), & LE^{A}(i,j)>LE^{B}(i,j) \\ L^{B}(i,j), & LE^{A}(i,j)<LE^{B}(i,j) \\ (L^{A}(i,j)+L^{B}(i,j))/2, & otherwise \end{cases} . \quad (12)$$

C. Fusion step

The fusion step occurs after the high-frequency and low-frequency coefficients fusion rule is designed. Assume that the medical images to be fused are coregistered to ensure that the corresponding pixels are aligned. The framework of the proposed fusion method is shown Fig. 3 and described in the following four steps. In Fig. 3, because the high-frequency coefficient is sparse, to enhance the visual effect each high-frequency coefficient is expanded three times.

1) Decompose the source images A and B by using the NSCT to obtain a series of high-frequency subbands at each level k and direction l and one low-frequency subband; that is, A: $\{H_{k,l}^{A},L^{A}\}$ and B: $\{H_{k,l}^{B},L^{B}\}$.

2) High-frequency fusion based on the type-2 fuzzy logic is applied to high frequency sub-images $H_{k,l}^{A}$ and $H_{k,l}^{B}$ to obtain $H_{k,l}^{F}$ following the procedure of Section III-A.

3) Fuse low-frequency subbands via the fusion rule based on the LE. Then obtain composite low-frequency subbands L^{F} following the procedure of Section III-B.

4) Use the inverse NSCT on the fused coefficients $\{H_{k,l}^{F},L^{F}\}$ to obtain the final fused medical image F.

D. Color image fusion

This subsection introduces an efficient color fusion scheme for colored sensor images. The PET and SPECT images can be treated as color images with the assumption that they are shown by pseudo-color. Fusion of gray and pseudo-color medical images presents more information of biological tissues in a single image. In the RGB color space, the three colors are equally treated and stored with the same resolution. Fusion modalities based on RGB inserted in three different channels are independent to some extent, so it can reduce blurred or missed gray details of fused image. However, this modality spoils the interpretation style of original palettes and increases the complexity of the fusion algorithm. [43]. Meanwhile, HVS for color is less sensitive than brightness. By separating the brightness and color information, a higher resolution for luminance values can be more effective to represent a color image.

YUV is a color space typically used as part of a color image

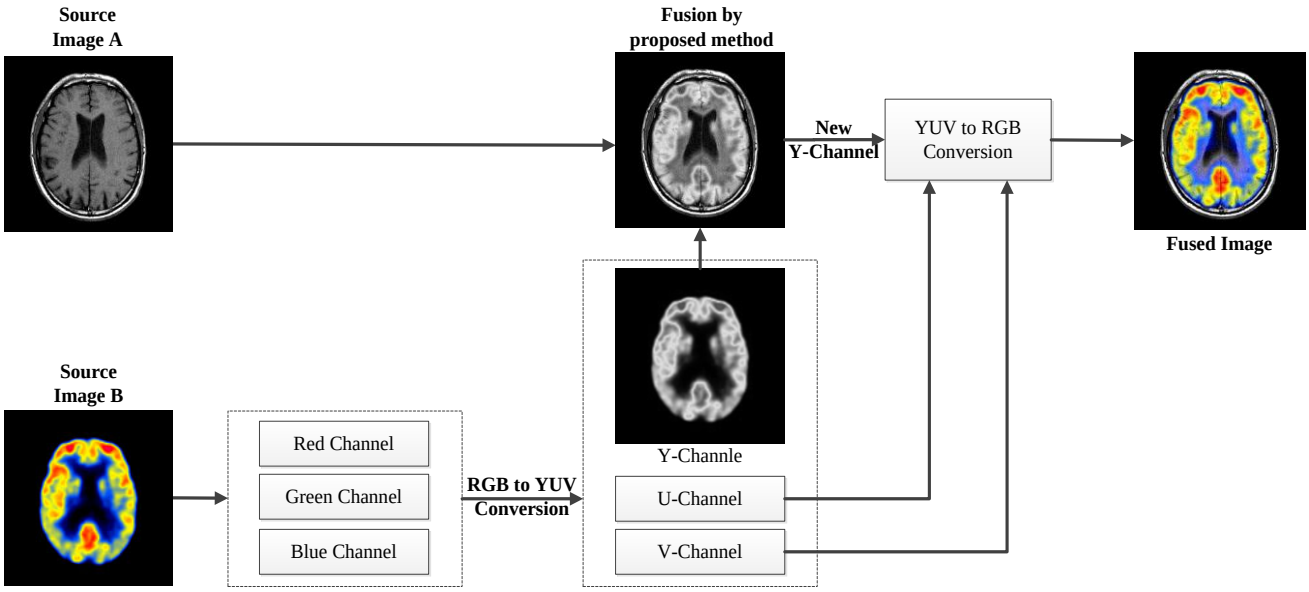

Fig. 4. The framework of the color image fusion: synchronization of proposed fusion algorithm in YUV color space.

This article has been accepted for publication in a future issue of this journal, but has not been fully edited. Content may change prior to final publication. Citation information: DOI 10.1109/JSEN.2016.2533864, IEEE Sensors Journal

pipeline. It is inspired by the color opponency theory in physiology, and encodes a color image or video taking into account human perception of achromatic and chromatic colors occurring in three independent dimensions [44]. The Y component determines the brightness of the color (referred to as luminance or luma), while the U and V components determine the color itself (the chroma). One tidy aspect of YUV is that we can discard the U and V components and get a gray scale image. As the gray scale and chrominance signals are disconnected, so we can change the intensity without affecting the colors of the case. Thus, the YUV is suitable for image fusion. The RGB to YUV color space conversion can be summarized as follows:

$$\begin{bmatrix} Y \\ U \\ V \end{bmatrix} = \begin{bmatrix} 0.299 & 0.587 & 0.114 \\ -0.169 & -0.331 & 0.5 \\ 0.5 & -0.419 & -0.081 \end{bmatrix} \begin{bmatrix} R \\ G \\ B \end{bmatrix}, \quad (13)$$

The inversion, YUV to RGB space, is done by the following inverse operations:

$$\begin{bmatrix} R \\ G \\ B \end{bmatrix} = \begin{bmatrix} 1 & 0 & 1.14 \\ 1 & -0.39 & 0.58 \\ 1 & 2.03 & 0 \end{bmatrix} \begin{bmatrix} Y \\ U \\ V \end{bmatrix}. \quad (14)$$

This scheme provides more contrast enhancement than do overlaying schemes because it fully utilizes color opponency in human perception. The core idea is to transform the color image from the RGB color space to the YUV color space using the process given above. Now, the gray scale image and the achromatic channel Y of the color image are fused using the proposed fusion algorithm, followed by the inverse YUV to RGB conversion to get the final fused image. The framework of the color image fusion method is shown Fig. 4.

IV. Experimental results and analysis

The presented fusion method is implemented and applied on clinically obtained different modality medical images. The medical images used in the research were obtained from http://www.imagefusion.org/ and http://www.med.harvard.edu /aanlib/home.html. To assess the performance of the proposed method, extensive experiments were carried out on nine different groups of medical images combining different modalities.

A. Evaluation criteria

In this step, the selected quantitative criteria used in objective analysis are described. It is well known that different image quality metrics measure the visual quality of images from different aspects, but none of them can directly measure the quality. In this paper, we consider both the visual representation and the quantitative assessment of the fused images. For evaluation of the proposed fusion method, we have considered three separate fusion performance metrics as defined below.

(1) Mutual information (MI): MI can indicate how much information the fused image conveys about the source images. MI between the fusion image and the source image is defined as follows [45]

$$MI = MI^{AF} + MI^{BF}, \quad (15)$$

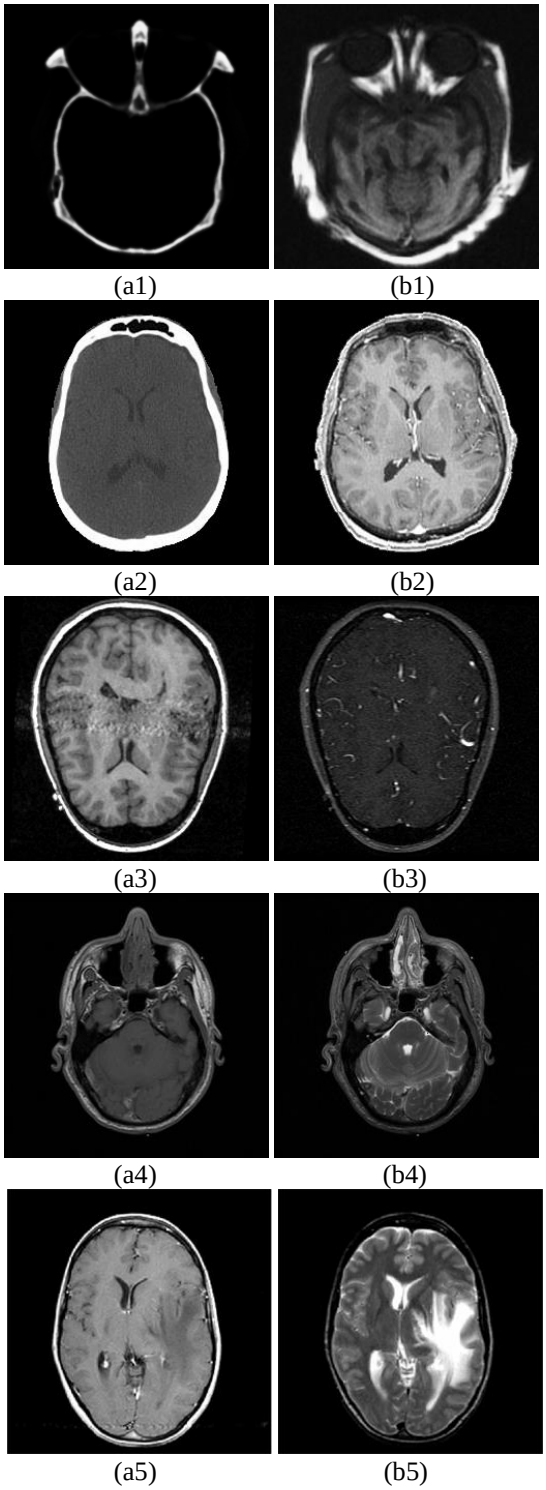

Fig. 5. Source multimodal medical images: (a1), (b1) image group 1 (CT and MRI); (a2), (b2) image group 2 (CT and MRI); (a3), (b3) image group 3 (MR-T1 and MRA); (a4), (b4) image group 4 (MR-T1 and MR-T2); (a5), (b5) image group 5 (MR-Gad and MR-T2).

in which

$$MI^{AF} = \sum_{f=0}^{L}\sum_{a=0}^{L} p^{AF}(a,f)\log_2\left(\frac{p^{AF}(a,f)}{p^{A}(a)p^{F}(f)}\right), \quad (16)$$

and

This article has been accepted for publication in a future issue of this journal, but has not been fully edited. Content may change prior to final publication. Citation information: DOI 10.1109/JSEN.2016.2533864, IEEE Sensors Journal

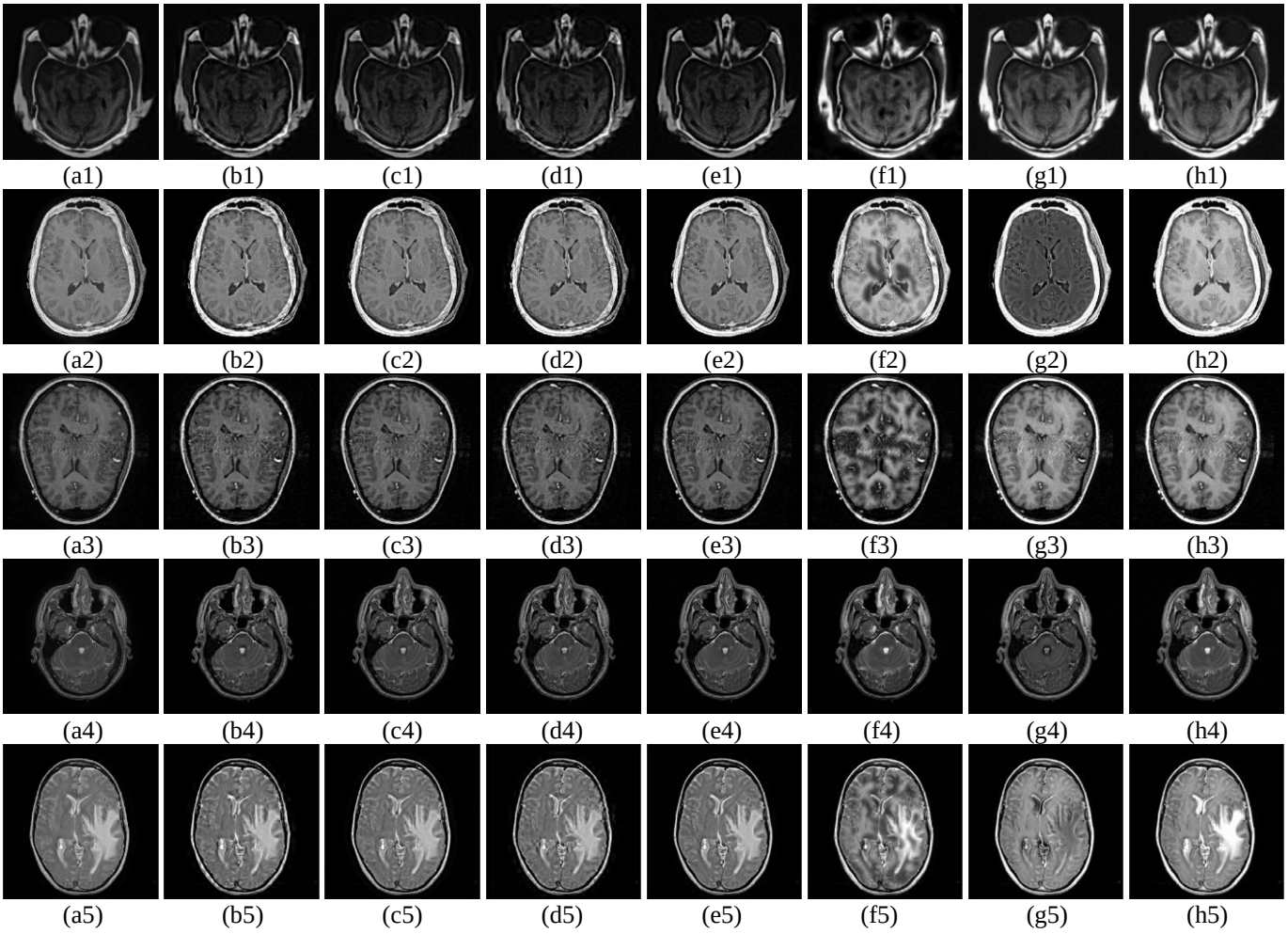

Fig. 6. Visual results for the five pairs of CT/MRI images. Fused images from (a1)–(a5) GP based method; (b1)–(b5) DWT based method; (c1)–(c5) DTCWT based method; (d1)–(d5) CT based method; (e1)–(e5) NSCT based method; (f1)–(f5) scheme [22] method; (g1)–(g5) scheme [27] method; (h1)–(h5) proposed method.

$$MI^{BF} = \sum_{f=0}^{L}\sum_{b=0}^{L} p^{BF}(b,f)\log_2\left(\frac{p^{BF}(b,f)}{p^{B}(b)p^{F}(f)}\right), \quad (17)$$

in which MI^{AF} and MI^{BF} denote the normalized MI between the fused image and the source images A and B; a, b and $f \in [0, L]$. $p^{A}(a)$, $p^{B}(b)$ and $p^{F}(f)$ are the normalized gray level histograms of the source images and the fused image. $p^{AF}(a,f)$ and $p^{BF}(b,f)$ are the joint gray level histograms between the fused image and the source images A and B. The greater the value of MI, the better the fusion effect.

(2) Edge Based Similarity Measure ($Q^{AB/F}$): $Q^{AB/F}$ which proposed by Xydeas and Petrovic [46] measures the similarity between the edges transferred from the source images to the fused image. The definition is given as

$$Q^{AB/F} = \frac{\sum_{i=1}^{M}\sum_{j=1}^{N}[Q^{AF}(i,j)w^{A}(i,j) + Q^{BF}(i,j)w^{B}(i,j)]}{\sum_{i=1}^{M}\sum_{j=1}^{N}[w^{A}(i,j) + w^{B}(i,j)]} \quad (18)$$

in which

$$Q^{AF}(i,j) = Q_a^{AF}(i,j)Q_g^{AF}(i,j) \quad (19)$$

$$Q^{BF}(i,j) = Q_a^{BF}(i,j)Q_g^{BF}(i,j), \quad (20)$$

where $w^{A}(i,j)$ and $w^{B}(i,j)$ are the corresponding gradient strengths for images A and B respectively. $Q_a^{xF}(i,j)$ and $Q_g^{xF}(i,j)$ are the edge strength and orientation preservation values at location (i,j) for each source image. Values of $Q^{AB/F}$ should be close to one, which indicates a better fused image.

(3) Standard Deviation (STD): The standard deviation can be used to estimate how widely spread the gray values are in an image. The larger the STD, the better the result. The STD is defined as:

$$STD = \left(\frac{1}{M\times N}\sum_{i=1}^{M}\sum_{j=1}^{N}\left(F(i,j) - \hat{\mu}\right)^2\right)^{1/2}, \quad (21)$$

where $F(i,j)$ is the pixel value of the fused image at the position (i,j) and $\hat{\mu}$ is the mean value of the image.

The visual and quantitative results for nine pairs of source images from the different combinations described previously are given in the next subsection. For simplicity, we have designated the nine pairs of source medical images as "group 1" to "group 9".

This article has been accepted for publication in a future issue of this journal, but has not been fully edited. Content may change prior to final publication. Citation information: DOI 10.1109/JSEN.2016.2533864, IEEE Sensors Journal

TABLE I
EVALUATION INDICES FOR FUSED MEDICAL IMAGES

Group	Indices	GP	DWT	DTCWT	CT	NSCT	Scheme [22]	Scheme [27]	Proposed method
Group 1 CT/MRI	*MI*	2.9816	2.3709	2.3663	2.1769	2.5573	2.6506	4.3924	**4.5619**
	$Q^{AB/F}$	0.6520	0.6180	0.6464	0.5763	0.6913	0.7014	**0.7889**	0.7859
	STD	38.7824	41.1599	39.7914	40.3183	41.2486	59.1884	58.2576	**60.8717**
Group 2 CT/MRI	*MI*	3.3544	3.1367	3.2059	3.1086	3.2943	3.2339	3.0614	**3.9635**
	$Q^{AB/F}$	0.5867	0.5670	0.5998	0.5541	0.6287	0.5942	0.5802	**0.6412**
	STD	68.3325	72.2603	70.9012	71.3378	72.2190	82.6464	72.1308	**90.1086**
Group 3 MR-T1/MRA	*MI*	3.8479	3.1827	3.3156	3.1689	3.4469	2.8063	4.5088	**4.6146**
	$Q^{AB/F}$	0.5665	0.5299	0.5631	0.5297	0.5926	0.5206	0.6268	**0.6469**
	STD	46.2356	50.8396	50.0670	50.4575	50.9719	57.6010	69.1269	**69.1941**
Group 4 MR-T1/T2	*MI*	3.5102	3.2095	3.2980	3.1454	3.4207	3.5195	3.5107	**4.0579**
	$Q^{AB/F}$	0.6632	0.6347	0.6742	0.6333	0.6862	0.6862	0.6641	**0.7154**
	STD	34.5850	37.3586	36.9695	37.3167	37.3700	40.4041	38.4298	**43.2922**
Group 5 MR-GAD/T2	*MI*	3.3656	3.1878	3.2148	3.1445	3.2716	3.3301	3.3819	**3.6634**
	$Q^{AB/F}$	0.5579	0.5266	0.5692	0.5190	0.5848	0.5755	0.5631	**0.6197**
	STD	62.5626	65.6693	64.7158	65.1074	65.4498	68.8262	70.1364	**80.0055**

B. Experiments on CT/MRI image fusion

This section, describes how we evaluated the performance of the proposed fusion approach by using five common groups of medical images combining different modalities (see Fig. 5). The images comprised two groups of CT and MRI images (CT/MRI), a group of T1-weighted MR image and magnetic resonance angiography (MR-T1/MRA), a group of MR-T1 and MR-T2 images (MR-T1/MR-T2), and a group comprising an MR image after Gd-DTPA and a T2-weighted image (MR-GAD /MR-T2).

The corresponding pixels of two input images were perfectly co-aligned by using the registration method from reference [47]. All images had the same size of 256 × 256 pixels, with a 256-level gray scale and 8-bit precision. We compared the performance of our technique with existing image fusion methods based on the GP, the DWT, the DTCWT, the CT and the NSCT. The high- and low-frequency coefficients of those methods were merged by the widely used fusion rule of selecting the coefficient with larger absolute values and the averaging rule respectively. In addition, our method was compared with the methods of references [22] and [27], which are all based on the NSCT. Method [22] proposed two different fusion rules based on directive contrast and phase congruency that are used to fuse high- and low-frequency coefficients. In the method [27], coefficients of both the high- and low-frequency subbands are fused in a similar way using reduced pulse coupled neural networks (RPCNNs) with fuzzy-adaptive linking strengths. To perform a fair comparison, the same experimental images were used for all existing methods. All the methods were the three layers decomposition. All the NSCT based methods had the same pyramidal and directional filters: "pyrexc" and "vk", respectively.

For the five image sets, the corresponding fusion results are given in Fig. 6. The first pair of medical images is two groups of brain CT and MRI images in different aspects. From the "group 1" fused image, it is clear that apart from our proposed method and the schemes of [22] and [27], the compared techniques suffered from contrast reduction. Moreover, it can be seen that the fused images obtained by the schemes of [22] lost many image details. On comparing the "group 2" results, it is clear that the proposed method outperformed the other fusion methods, and its fused image has good visual representation of both bone structure and soft tissue information. On observing the "group 3", one can see the lesions and their vascular properties, and the soft tissue information is apparent in the fused images of the proposed scheme and the schemes of [27]. However, "group 4" clearly shows that the fused images of the proposed scheme and the schemes of [22] have better quality and contrast than those of the other methods. This shows the limitations of the schemes of [22] and [27], which are not suitable for some common multimodal medical images. Finally, after observation of the "group 5", we can see that the features and detailed information presented in the proposed method's fused image are much richer than those of the other fused images. The image content, such as tissues are clearly enhanced. The analysis above verifies that the proposed method was superior to other fusion methods in visual representation.

In addition to the subjective analysis, we conducted a detailed objective analysis on the above experimental results by different fusion methods. For the five pairs of medical images, quantitative performance comparisons of our proposed method with other schemes are given in the Table I. In the Table I, the proposed method's two values of the MI and STD are the largest objective measures, and the $Q^{AB/F}$ is 0.7859, which is very close to the highest value, 0.7889. The highest values of MI indicate that the fused images obtained by the proposed

This article has been accepted for publication in a future issue of this journal, but has not been fully edited. Content may change prior to final publication. Citation information: DOI 10.1109/JSEN.2016.2533864, IEEE Sensors Journal

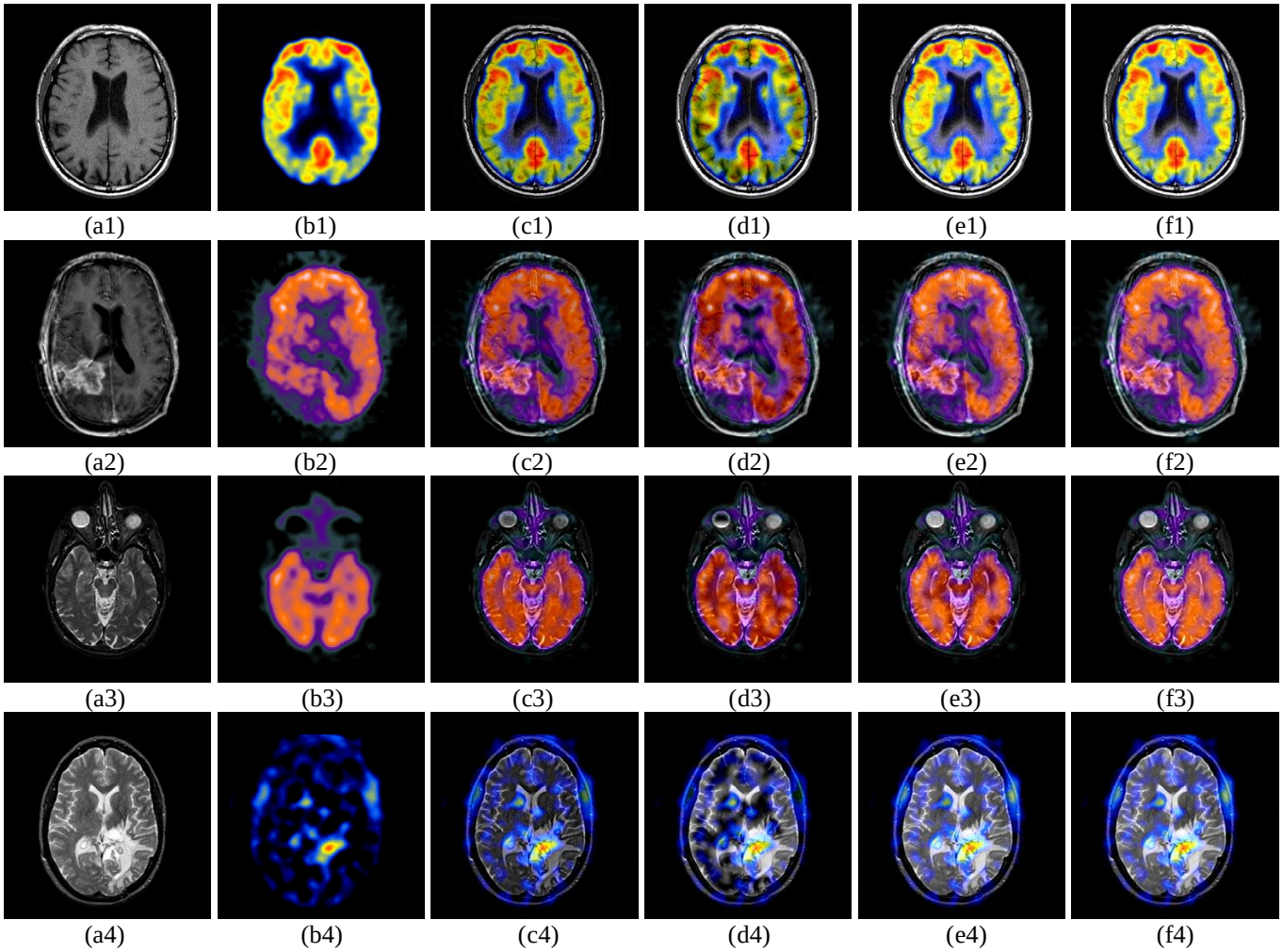

Fig. 7. Group 6 through Group 9 source multimodal medical images and results: (a1)–(a4) MRI images. (b1) and (b2) PET images. (b3) and (b4) SPECT images. (c1)–(c4) by NSCT method, (d1)–(d4) by scheme [22] method, (e1)–(e4) by scheme [27] method, (f1)–(f4) by proposed method.

method conveyed more information about the source images than did the other methods. Similarly, the higher values of STD for the proposed method fused images show they had higher contrast than the other schemes. At the same time, it is clear from the previous five methods that NSCT based method is superior to the DWT, DTCWT, and CT based methods. Compared with the GP based method, although the MI of NSCT is slightly less than its value, the advantages of the $Q^{AB/F}$ and STD are obvious. Therefore, in general, the NSCT based method is better than the other four multiresolution based algorithms. If the three NSCT based methods are compared it can be seen that the performance of the proposed method is better than existing NSCT based methods [22] and [27]. At the same time, objective evaluation shows that the versatility of methods [22] and [27] is not good. Method [27] in the "group 1" and "group 3" experiments was significantly better than method [22], but for the "group 2" and "group 4" experiments, method [22] was better than method [27]. By comparison, the proposed fusion rules for high- and low-frequency coefficients can effectively extract prominent and detailed information from the various types of source images.

C. Experiments on PET/MRI and SPECT/MRI image fusion

Despite the great success of CT-MRI fusion, its role in neuroscience is considered to be limited compared with the potential of PET/MRI and SPECT/MRI fusions. This is because PET/MRI and SPECT/MRI fusions are analyzed over CT-MRI fusion for better diagnoses in various diseases. To demonstrate the significant performance of the proposed scheme, more elaborate performance comparison analysis was done with brain images in group 6 through 9. Each scan contains 256 × 256 pixels with 8-bit precision in the luminance channel. The fusion results were compared with the best three NSCT based algorithms used in the earlier analysis.

The first two examples of MRI/PET fusion images contain one MRI scan and one color PET scan of a brain. As displayed in Fig. 7 (c1) through (f1) and (c2) through (f2), the metabolic activity revealed in the PET scan and the anatomical structures revealed in the MRI scan are combined in the fused image, providing the best spatial relationships of our method. The second two examples of MRI/SPECT fusion images contain one MRI scan and one color SPECT scan. In Fig. 7 (f3), it is found that the brain structures are fully preserved in the

non-functional area, while the color information of the SPECT image can be well located by MRI details in the functional area. As demonstrated in Fig. 7 (c4) through (f4), our method combined the high Thallium uptake shown in the SPECT scan with the anatomical structures shown in the MRI scan in the fused image for better determination of the extent of the tumor, while preserving high image contrast.

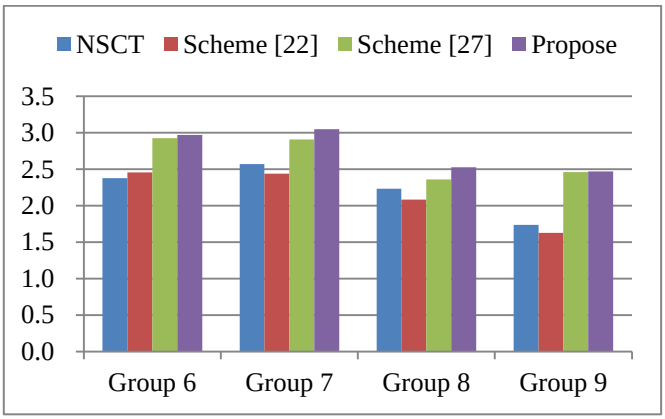

(a) MI

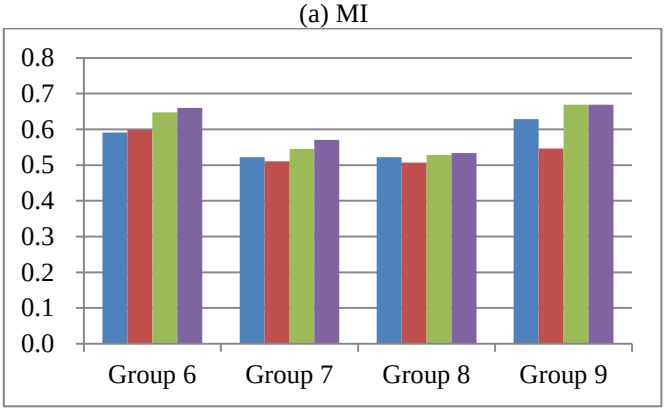

(b) $Q^{AB/F}$

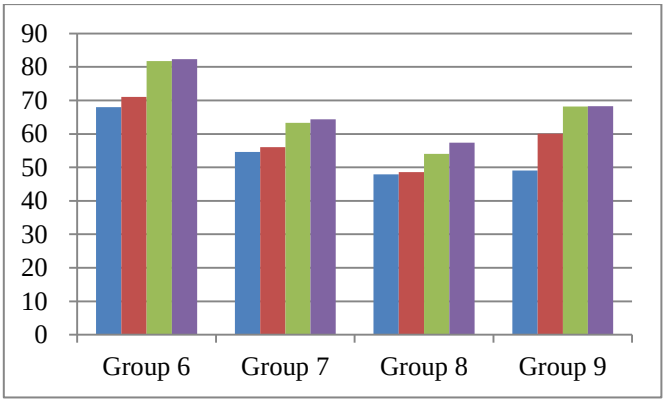

(c) STD

Fig. 8. The evaluation metrics for color fused images

Besides the visual comparison, we also compared the proposed method with other three other fusion algorithms under different metrics. These evaluation indices were defined for gray scale images, and the PET/SPECT image is a color image. Therefore, the metrics were evaluated with each color channel in turn, and then the average of all values was taken as the final result. The results are shown in Fig. 8; in general, the proposed method had higher evaluation indices than the other methods.

Hence, it is obvious from Figs. 6-8, and Table I that both the visual and statistical evaluations demonstrated that the fused images obtained by the proposed method based on the NSCT and type-2 fuzzy logic were more informative, were clearer, and had higher contrast than existing methods.

V. Conclusion

In this paper, a novel multimodal sensor medical image fusion method based on type-2 fuzzy logic in NSCT domain is proposed. To overcome the limitations of the traditional fusion methods, a new couple of fusion rules based on type-2 fuzzy logic and LE are used to preserve more useful information and improve the quality of the fused images. Experimental results clearly demonstrate that the proposed algorithm can enhance the details of the fused image and can improve the visual effect with less difference to the source images than several popular widely used fusion methods. Simultaneously, the better experimental results of color image fusion highlighting the strong efficiency of the proposed method. In the future work, we will focus on extending a generalized fuzzy logic based fusion methods into other areas of applications.

References

[1] L. Wang, B. Li, and L. Tian, "Multimodal medical volumetric data fusion using 3-D discrete shearlet transform and global-to-local rule," *IEEE Trans. Biomed. Eng.*, vol. 61, no. 1, pp. 197–206, 2014.

[2] X. U. Zhiping, "Medical image fusion using multi-level local extrema," *Inf. Fusion*, vol. 19, no. 11, pp. 38–48, 2013.

[3] Q. Wang, S. Li, H. Qin, and A. Hao, "Robust multi-modal medical image fusion via anisotropic heat diffusion guided low-rank structural analysis," *Inf. Fusion*, vol. 26, pp. 103–121, 2015.

[4] R. Singh, R. Srivastava, O. Prakash, A. Khare, and R. Srivastava, "Multimodal Medical Image Fusion in Dual Tree Complex Wavelet Transform Domain Using Maximum and Average Fusion Rules," *J. Med. Imaging Health Inf.*, vol. 2, no. 2, pp. 168–173, 2012.

[5] R. Singh, and A. Khare, "Fusion of multimodal medical images using Daubechies complex wavelet transform – A multiresolution approach," *Inf. Fusion*, vol. 19, no. 3, pp. 49–60, 2014.

[6] A. P. James, and B. V. Dasarathy, "Medical Image Fusion: A survey of the state of the art," *Inf. Fusion*, vol. 19, no. 3, pp. 4–19, 2013.

[7] E. Andreas, C. L. Pagliari, and E. A. B. Silva, Da, "Multiscale image fusion using the undecimated wavelet transform with spectral factorization and nonorthogonal filter banks," *IEEE Trans. Image Process.*, vol. 22, no. 3, pp. 1005–1017, 2013.

[8] R. Redondo, F. Šroubek, S. Fischer, and G. Cristóbal, "Multifocus image fusion using the log-Gabor transform and a Multisize Windows technique,"*Inf. Fusion*, vol. 10, no. 2, pp. 163–171, 2009.

[9] P. Balasubramaniam, and V. P. Ananthi, "Image fusion using intuitionistic fuzzy sets," *Inf. Fusion*, vol. 20, no. 15, pp. 21–30, 2014.

[10] Y. Yang, S. Tong, S. Huang, and P. Lin, "Multifocus Image Fusion Based on NSCT and Focused Area Detection," *IEEE Sensors J.*, vol. 15, no. 5, pp. 2824–2838, 2015.

[11] Y. Liu, S. Liu, and Z. Wang, "A general framework for image fusion based on multi-scale transform and sparse representation," *Inf. Fusion*,vol. 24, pp. 147–164, 2015.

[12] V. S. Petrovic, and C. S. Xydeas, "Gradient-based multiresolution image fusion," *IEEE Trans. Image Process.*, vol. 13, no. 2, pp. 228–237, 2004.

[13] S. M. M. Rahman, M. O. Ahmad, and M. N. S. Swamy, "Contrast-based fusion of noisy images using discrete wavelet transform," *IET Signal Process.*,vol. 4, no. 5, pp. 374–384, 2010.

[14] M. Yin, W. Liu, X. Zhao, Y. Yin, and Y. Guo, "A novel image fusion algorithm based on nonsubsampled shearlet transform," *Optik—Int. J. Light Electron Opt.*, vol. 125, no. 10, pp. 2274–2282, 2014.

[15] N. G. Kingsbury, "The dual-tree complex wavelet transform: a new technique for shift invariance and directional filters." in *Proc. Eighth IEEE DSP Workshop*, 1998.

[16] Y. Chai, H. Li, and X. Zhang, "Multifocus image fusion based on features contrast of multiscale products in nonsubsampled contourlet transform domain," *Optik—Int. J. Light Electron Opt.*, vol. 123, no. 7, pp. 569–581, 2012.

[17] M. N. Do, and V. Martin, "The contourlet transform: an efficient directional multiresolution image representation," *IEEE Trans. Image Process.*, vol. 14, no. 12, pp. 2091–2106, 2005.

[18] L. Yang, B. L. Guo, and W. Ni, "Multimodality medical image fusion based on multiscale geometric analysis of contourlet transform," *Neurocomputing*, vol. 72, pp. 203–211, 2008.

[19] A. L. D. Cunha, J. Zhou, and M. N. Do, "The Nonsubsampled Contourlet Transform: Theory, Design, and Applications," *IEEE Trans. Image Process.*, vol. 15, no. 10, pp. 3089–3101, 2006.

[20] W. Kong, Y. Lei, and X. Ni, "Fusion technique for grey-scale visible light and infrared images based on non-subsampled contourlet transform and intensity–hue–saturation transform," *IET Signal Process.*, vol. 5, no. 1, pp. 75–80, 2011.

[21] Q. Zhang, and B. L. Guo, "Multifocus image fusion using the nonsubsampled contourlet transform," *Signal Process.*, vol. 89, pp. 1334–1346, 2009.

[22] G. Bhatnagar, Q. M. J. Wu, and Z. Liu, "Directive contrast based multimodal medical image fusion in NSCT domain," *IEEE Trans. Multimedia*, vol. 15, no. 5, pp. 1014–1024, 2013.

[23] G. Liu, Y. Zhang, and A. Wang, "Incorporating adaptive local information into fuzzy clustering for image segmentation," *IEEE Trans. Image Process.*, vol. 24, pp. 3990–4000, 2015.

[24] A. T. Celebi, R. Duvar, and O. Urhan, "Fuzzy fusion based high dynamic range imaging using adaptive histogram separation," *IEEE Trans. on Consum. Electron.*, vol. 61, no. 1, pp. 119–127, 2015.

[25] F. D. Martino, P. Hurtik, I. Perfilieva, and S. Sessa, "A color image reduction based on fuzzy transforms," *Inf. Sci.*, vol. 266, no. 2, pp. 101–111, 2014.

[26] J. K. Udupa, D. Odhner, L. Zhao, Y. Tong, M. M. S. Matsumoto, K. C. Ciesielski, A. X. Falcao, P. Vaideeswaran, V. Ciesielski, and B. Saboury, "Body-wide hierarchical fuzzy modeling, recognition, and delineation of anatomy in medical images," *Med. Imag. Anal.*, vol. 18, no. 5, pp. 752–771, 2014.

[27] D. S, and K. MK, "A Neuro-Fuzzy Approach for Medical Image Fusion," *IEEE Trans. Biomed. Eng.*, vol. 60, no. 12, pp. 3347–3353, 2013.

[28] M. E. Yüksel, and M. Borlu, "Accurate Segmentation of Dermoscopic Images by Image Thresholding Based on Type-2 Fuzzy Logic," *IEEE Trans. Fuzzy Syst.*, vol. 17, no. 4, pp. 976–982, 2009.

[29] P. Melin, C. I. Gonzalez, J. R. Castro, O. Mendoza, and O. Castillo, "Edge Detection Method For Image Processing Based On Generalized Type-2 Fuzzy Logic," *IEEE Trans. Fuzzy Syst.*, vol. 22, no. 6, pp. 1515–1525, 2014.

[30] T. N. Long, D. S. Mai, and W. Pedrycz, "Semi-supervising Interval Type-2 Fuzzy C-Means clustering with spatial information for multi-spectral satellite image classification and change detection," *Comput. & Geosci.*, vol. 83, pp. 1–16, 2015.

[31] I. De, "No-reference image quality assessment using interval type 2 fuzzy sets," *Appl. Soft Comput.*, vol. 30, pp. 441–453, 2015.

[32] M. T. Yildirim, A. Basturk, and M. E. Yuksel, "Impulse Noise Removal From Digital Images By A Detail-Preserving Filter Based On Type-2 Fuzzy Logic," *IEEE Trans. Fuzzy Syst.*, vol. 16, no. 4, pp. 920–928, 2008.

[33] L. A. Zadeh, "Fuzzy sets," *Inf. and control*, vol. 8, no. 3, pp. 338–353, 1965.

[34] J. M. Mendel, and R. I. B. John, "Type-2 fuzzy sets made simple," *IEEE Trans. Fuzzy Syst.*, vol. 10, no. 2, pp. 117–127, 2002.

[35] Q. Liang, and J. M. Mendel, "Interval type-2 fuzzy logic systems: theory and design," *IEEE Trans. Fuzzy Syst.*, vol. 8, no. 5, pp. 535–550, 2000.

[36] G. Bhatnagar, Q. M. J. Wu, and Z. Liu, "A New Contrast based Multimodal Medical Image Fusion Framework," *Neurocomputing*, vol. 157, pp. 143–152, 2015.

[37] L. A. Zadeh, "Probability measures of Fuzzy events," *J. Math. Anal. Appl.*, vol. 23, no. 2, pp. 421-427, 1968.

[38] L. Li, D. Li, "Fuzzy entropy image segmentation based on particle swarm optimization," *Progr. Nat. Sci.*, vol. 18, no. 9, pp. 1167–1171, 2008.

[39] H. R. Tizhoosh, "Image thresholding using type II fuzzy sets," *Pattern Recognit.*, vol. 38, no. 12, pp. 2363-2372, 2005.

[40] D. Wu, and J. M. Mendel, "Uncertainty measures for interval type-2 fuzzy sets," *Inf. Sci.*, vol. 177, no. 23, pp. 5378–5393, 2007.

[41] W. Zeng, and H. Li, "Relationship between similarity measure and entropy of interval valued fuzzy sets," *Fuzzy Sets & Syst.*, vol. 157, no. 11, pp. 1477–1484, 2006.

[42] T. Q. Deng, Z. J. Wang, P. P. Wang, and C. D. Sheng, "Study on fuzzy entropy of type-2 fuzzy sets," *Control & Decision*, vol. 27, no. 3, pp. 408–412, 2012.

[43] T. Li, Y. Wang, C. Chang, N. Hu, Y. Zheng, "Color-appearance-model based fusion of gray and pseudo-color images for medical applications," *Inf. Fusion*, vol. 19, no. 6, pp. 103–114, 2014.

[44] S. Rui, C. Irene, and B. Anup, "Cross-scale coefficient selection for volumetric medical image fusion," *IEEE Trans. Biomed. Eng.*, vol. 60, no. 4, pp. 1069–1079, 2013.

[45] G. Qu, D. Zhang, and P. Yan, "Information measure for performance of image fusion," *Electron. Lett.*, vol. 38, no. 7, pp. 313–315, 2002.

[46] C. Xydeas, and V. Petrović, "Objective image fusion performance measure," *Electron. Lett.*, vol. 36, no. 4, pp. 308–309, 2000.

[47] A. Sotiras, C. Davatzikos, and N. Paragios, "Deformable medical image registration: A survey," *IEEE Trans. Med. Imag.*, vol. 32, no. 7, pp. 1153–1190, Jul. 2013.